The Role of Shape on Electronic Structure and Charge Transport in Faceted PbSe Nanocrystals

Ananth P. Kaushik, Binit Lukose, and Paulette Clancy*

School of Chemical and Biomolecular Engineering, Cornell University, Ithaca, New York 14853, United States

ABSTRACT We have determined the effect of shape on the charge transport characteristics of nanocrystals. Our study looked at the explicit determination of the electronic properties of faceted nanocrystals that essentially probe the limit of current computational reach, *i.e.*, nanocrystals from 1.53 to 2.1 nm in diameter. These nanocrystals, which resemble PbSe systems, are either bare or covered in short ligands. They also differ in shape, octahedral *vs* cube-octahedral, and in superlattice symmetry (fcc *vs* bcc). We have provided insights on electron and hole coupling along different facets and overall charge mobility in bcc and fcc superlattices. We have determined that the relative areas of (100) to (111) facets, and facet atom types are important factors governing the optimization of charge transport. The calculated electronic density of states shows no role of $-SCH_3^-$ ligands on states near the band gap. Electron coupling between nanocrystals is significantly higher than that of hole coupling; thiol ligands lower the ratio between electron and hole couplings. Stronger coupling exists between smaller nanocrystals.

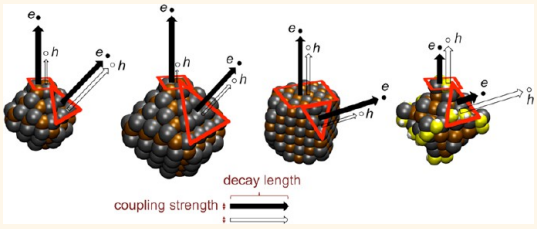

KEYWORDS: quantum dots · density functional theory · density of states · charge transfer · Marcus theory

Quantum dots (or nanocrystals) exhibit the defining characteristic that their properties are controlled by their size and are different from their bulk counterparts in a manner inconsistent with mere scaling.[1−6] Interest in nanocrystal (NC) assemblies arises from a variety of applications, including solar cells,[1−5,7−12] field effect transistors,[13−15] light-emitting diodes,[16,17] photodetectors,[18] and chemical sensors.[19] In this paper, we focus on colloidal NCs, which can be easily solution-processed and drop-cast onto suitable substrates to provide an inexpensive method of producing electronic devices.[20,21] NCs formed from lead salts, such as PbSe, PbTe, PbS *etc.*, have received considerable attention in recent years,[1−5] mainly due to their large Bohr exciton radius and narrow, yet size-tunable, band gaps.[22] Their ability to provide significant electronic coupling at close proximity[23] and to self-assemble into a variety of large two- and three-dimensional superlattices[20,21,24] makes them ideally suited for use in photovoltaic devices and other optoelectronic applications.[11,12,14,15]

Exploiting the unique nanocrystal properties of NCs in effective electronic devices is currently constrained by our lack of understanding of charge transport. Transport is determined by a complex and interacting set of variables: the size distribution of the NCs, surface chemistry and stoichiometry, morphological order, and inter-NC distances. The long-chain alkyl ligands that are invariably employed to prevent NC sintering also play a role in determining charge transport characteristics of NCs, in terms of physical intervention that deleteriously increases the inter-NC separation and by inserting a medium through which charge has to travel, creating a tunneling barrier. This has led to the use of shorter chains and conducting ligands. One dramatic example of this was the use of the short connector hydrazine in PbSe NC thin films which improved the mobilities by orders of magnitude.[15] Similar improvements were seen using other short connectors, 1,2-ethanedithiol[11] and $Sn_2S_6^{4-}$.[25] Embedding PbSe NCs in a matrix of CdSe NCs affixed to a substrate to form molecular aggregates also showed promise.[26] Most recently, Kagan *et al.* has shown that compact ammonium thiocyanate ligands on PbX NCs can promote impressive electron mobilities (on the order of 10 $cm^2/(V\ s)$) while retaining quantum confinement.[27,28]

* Address correspondence to pc@icse.cornell.edu.

Received for review November 5, 2013 and accepted February 18, 2014.

Published online February 18, 2014
10.1021/nn405755n

The effect of NC *shape* is often invoked in this discussion as being important, but actually *uncovering the nature of its role* in charge transport processes has achieved little attention. This is not surprising since it is difficult to tease apart the contribution of shape alone from among the many variables that contribute to experimental observations. This provided the motivation for our computational study.

This paper presents a detailed DFT study of the full electronic structure and charge transport characteristics of small, close to realistically sized, PbSe NCs in bare *and* ligand-clad NCs (without pseudopassivation). This obviates any need to stitch together approximations for different aspects of the calculations, an approach used in past studies. While we have chosen PbSe as a test case, such a DFT analysis is clearly not limited to this system alone. Indeed, we have performed simulations of PbS NCs and found the electronic structure of both PbS and PbSe NCs to be very similar. The largest NC we have studied is 2.1 nm in diameter. While this is well below the size typically studied in experiments (3−10 nm), larger NCs are outside the limit of current computational means without a heroic effort. The insights that we provide for this small NC should, we suggest, be equally relevant for larger diameter NCs.

Our paper will show that the effect of the shape of the NC is more important than size in determining the distribution of charge densities in the NC and hence charge transport. The qualitative trends obtained in this study can be used to guide charge transport calculations for larger NCs composed of any PbX material and, further, the design of self-assembled superlattices of faceted NCs in general.

Our primary system considered a 1.53 nm diameter $Pb_{40}Se_{40}$ NC containing 80 atoms, which is easily accessible to a DFT study. The shape of this primary system NC was an octahedron, but we have also simulated a 1.53 nm *cube-octahedral* NC (184 atoms), which has the same [111] facet area as the octahedral NC, but larger [100] facet area. This comparison allows us to study the effect of shape of the NCs on charge transport properties without the complication of differing facet sizes. Comparison to a larger, 2.1 nm, NC provides estimates of the effect of NC size. We begin with a study of surface reconstructions on the NC and the binding of ligands to the surface of the reconstructed NC. Reconstruction strongly relaxes the NCs.[29] In this regard, Bealing *et al.* have shown that *un*reconstructed PbSe NC surfaces are not energetically viable to bind ligands on the facets considered here.[30] This leads to a study of the electronic coupling between two NCs and the determination of electron and hole transfer rates between them. We then calculate charge coupling and transfer rates for *bare* NCs of different shapes (to study the effect of shape) and also for *ligand-clad* NCs (in order to study the effect of ligands on charge transport). We also calculate electron and hole mobilities in an fcc and a bcc superlattice of NCs to compare charge transport in different superlattice symmetries.

The computational complexity of studying charge transfer in NCs has often led to approximations of the structure of the NCs in some manner or another. For example, considering them as a truncated bulk crystal or those whose surface pseudoatoms have been passivated. For example, Luo *et al.* studied the manner of decay of highly excited electrons in truncated bulk semiconductor crystals, used to approximate NCs, and introduced a figure of merit for carrier multiplication that differentiated between chalcogenide materials like CdSe and PbSe.[31] Franceschetti *et al.* studied carrier localization due to confinement *versus* electron correlation in semiconductor nanodumbbells, showing that dumbbell shape and size affected localization.[32] An *et al.* studied excitonic splitting and radiative lifetime in *spherical* PbSe NCs using configuration interaction methods.[33,34] Califano *et al.* studied hole relaxation in CdSe NCs and showed how the size and aspect ratio of nanostructures, such as nanorods, affected hole relaxation.[35] All these studies use empirical pseudopotentials to model the electronic structure, which are more efficient, but potentially less transferrable than density-functional theory (DFT). Ligand pseudopotentials at the surface provide passivation. This approach is computationally efficient enough to overcome the cost of using larger ligand-passivated NCs, but neglects the effects of the specific ligand chemistry and the contribution of ligands to the total electronic structure of the NC. Studies by Talapin *et al.* have shown that ligand chemistry is important in determining charge transfer in NC systems.[15]

There have been many *ab initio* studies of NCs of Si, CdSe, CdTe, and PbSe. Kiran *et al.* used DFT to find that $(PbS)_{32}$ was the smallest cubic cluster for which its inner $(PbS)_4$ core exhibits bulk-like coordination.[36] This helps provide a rubric for understanding the pattern of aggregation when $(PbS)_{32}$ clusters are deposited on a suitable surface. The existence, or not, of gap states is important in determining electronic properties and thus it is not surprising that this aspect has received some attention: For example, Gai *et al.*'s studies of structural and electronic properties of nonstoichiometric PbSe NCs hypothesized that dangling bonds may be responsible for introducing gap states.[37] In contrast, Voznyy claimed that it is ligands, rather than dangling bonds, that are responsible for surface traps and gap states.[38] There have also been DFT and time-dependent DFT (TD-DFT) studies of the role of different ligand chemistries and solvents on the electronic structure of CdSe NCs.[39] More recently, there have also been studies of multiexciton generation and hot carrier relaxation in Si and PbSe NCs using *ab initio* methods.[40,41]

The "cost" of using *ab initio* computational approaches to study charge transport in NCs is sufficiently

high that, in practice, it essentially limits the study of such systems to those containing less than a few hundred atoms. This difficulty was encountered in a recent study of charge transport between two spherical CdSe NCs linked by a compact $Sn_2S_6^{4-}$ connector.[42] Chu *et al.* studied charge transport in impressively large 2.5−5 nm diameter *spherical* NC dimer systems which involved using electronic structure calculations for a representative motif of the spherical NC linked to a set of other theoretical models to represent charge hopping.[42] This study made predictions of the effect of NC size and temperature on mobility that, for now, await experimental confirmation. However, this study did not take into account the effect of shape of the NCs on the charge transport, which is our focus here.

Past *ab initio* studies of NCs thus roughly fall into two categories: either they involve assumptions about the ligand coverage and the electronic structure (using pseudopotentials)[31−35] when charge hopping is considered, or else charge transport calculations are not performed if the actual ligand bonding is simulated and full *ab initio* methods are used, allowing calculations of the density of states (DOS) and a description of the structure of the NCs.[36−42]

RESULTS AND DISCUSSION

The structure of a bare, relaxed 1.53 nm NC is shown in the Supporting Information in Figure S1. We find the lattice constant near the core of the NC to be approximately the same as that of bulk PbSe, but the lattice constant at the surface, 0.605 nm, is slightly smaller than the bulk value of 0.612 nm. This phenomenon has also been observed by Franceschetti *et al.*[43,44] This difference arises from the fact that the surface of the NC is unpassivated and hence the surface energy (essentially a surface tension) is unable to take advantage of the stabilization provided by the ligands.

Density of States. We began by calculating the density of states of bare (Figure 1) and ligand-clad (Figure 2) NCs using the HSEh1PBE functional in conjunction with the split basis sets of LANL2DZ/6-31+G(d,p) for the core and ligands, respectively. The projected density of states (PDOS) for the bare 1.5 nm octahedral NC is plotted in Figure 1a. The valence orbital (HOMO) of the NC is formed predominantly from Se p states, whereas the LUMO consists of Pb p states. The corresponding localization of the holes on Se and electrons on Pb atoms is visible in the orbital plots of the HOMO and LUMO shown, respectively, in panels a and b of Figure 3. Isosurfaces for the wave functions have been plotted at an isovalue of 0.0075. Blue and red isosurfaces correspond to the positive and negative parts of the wave function, respectively.

On the bare NC, the HOMO and LUMO are delocalized and form p-like envelopes, on Se and Pb, respectively, as shown in Figure 3a. This is in agreement with the findings of Gai *et al.*[37] and Voznyy[38] for fellow chalcogenide CdSe NCs where the valence states are comprised of Se p states and the conduction states are comprised of Cd s states.

In our system, both the valence and conduction states are similar and are not very dense. The PDOS for the *bare* NCs are suggestively *mirror-symmetric* on both sides of the band gap. This symmetry confirms an early suggestion by Kang and Wise in 1997.[45] Kang and Wise's result was later contested by others who studied *spherical* NCs, for example, see references.[33,34,43,46] Despite these papers, and others, the subject of the symmetry, or not, of the PDOS of *spherical* nanocrystals remains a matter of debate. Some STM experiments for PbSe NCs[26] have confirmed the early work;[45] however, more recent work shows asymmetric optical transitions.[46,47] Note that not all chalcogenides show symmetric DOS: In CdSe NCs, for example, Yu *et al.*'s DFT calculations show asymmetric valence and conduction states, and the valence states appear to be far denser than the conduction states.[48] Even for our results, the determination of symmetry is somewhat ambiguous: While the HOMO and LUMO appear symmetric for the energy range given in Figure 1, if we investigate the *immediate neighborhood* of the band gap, not only are they somewhat unsymmetrical, but the densities of valence and conduction bands are different. Whether the PDOS is symmetric or not is important for exciton dissociation and recombination rates. It is more difficult for excitons to decay if both the conduction and valence states are equally sparse, giving rise to longer exciton life times. If the valence states are denser than the conduction states, electrons can transfer energy to the hole, and the hole could relax easily in the dense valence states. However, Figure 1 shows that filled and empty states near band edges are not equally sparse due to the nonuniform distribution of valence and conduction states (see Figure 3b). Deconstructing the factors affecting the symmetry of the PDOS is important; however, it is not the focus of this paper.

Our results for 1.5 nm bare, 2.1 nm bare, and 1.5 nm ligand-clad octahedral nanocrystals (Figure 1a, Figure 1c, and Figure 2, respectively) each show small peaks isolated from the conduction band. To see if these isolated peaks can be ascribed to surface traps, we projected the DOS of a 1.53 nm octahedral NC onto Pb atoms on different surfaces. As shown in Figure S3, the isolated peaks have contributions from Pb atoms on both [100] and [111] surfaces, as well as from inner Pb atoms. In other words, the state is not locally focused, as would be the case for a trap. Contributions to the DOS are proportional to the respective number of atoms in each region. Our data show that the isolated peak is *not* a trap state.

We turn now to the effect of including ligands on the PDOS by covering specific facets with CH_3S^- ligands. The experimental trend toward using shorter ligands on the NC surface, and hence surface

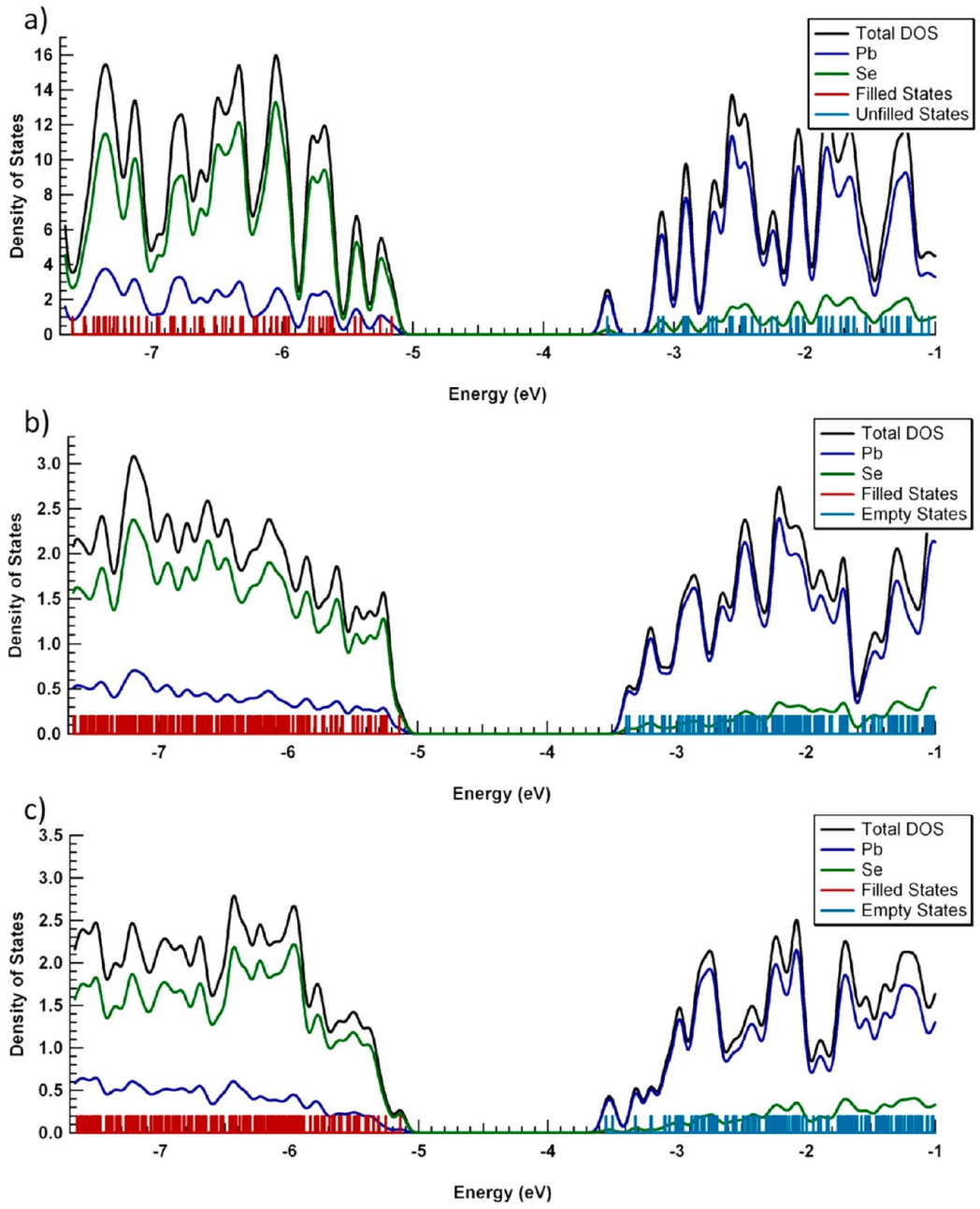

Figure 1. Projected density of states of bare PbSe NCs: (a) 1.5 nm octahedral NC (individual orbital energies are also shown); (b) 1.5 nm cube-octahedral NC; (c) 2.1 nm octahedral NC. A 100 meV Gaussian broadening of peaks has been used.

modification, can lead to an increased tendency for trap formation. For example, Ip *et al.* showed that loss of ligands reduces the coordination of the surface atoms and increases the likelihood of creating trap states.[49] However, our projected DOS calculations, explained below, indicate that ligands do not necessarily modify the optical properties, as they have no contributions near the band gap.

Our results are shown for cases in which either the [100] (Figure 2a) or [111] (Figure 2b) surface is covered with SCH_3^- ligands. These figures show that ligand-related levels in the NC remain deep in the valence and conduction orbitals and their significant broadening compared to a free ligand molecule indicates strong mixing with PbSe. Ligand contribution to the frontier orbitals (HOMO and LUMO) and the isolated states is negligible; most of the contribution comes from the core atoms of Pb and Se. This can be seen in the isosurface orbital plots of the HOMO of the ligand-clad NC in Figure 3c (for isovalue = 0.003). Note that the isovalues used in Figure 3a,c are different in order to make clear the nature of the localization over the ligand. The HOMO is localized over the Se atoms and the LUMO over the Pb atoms. The wave functions are primarily deep in the core of the NC and are not delocalized over the ligand atoms, so the ligands are

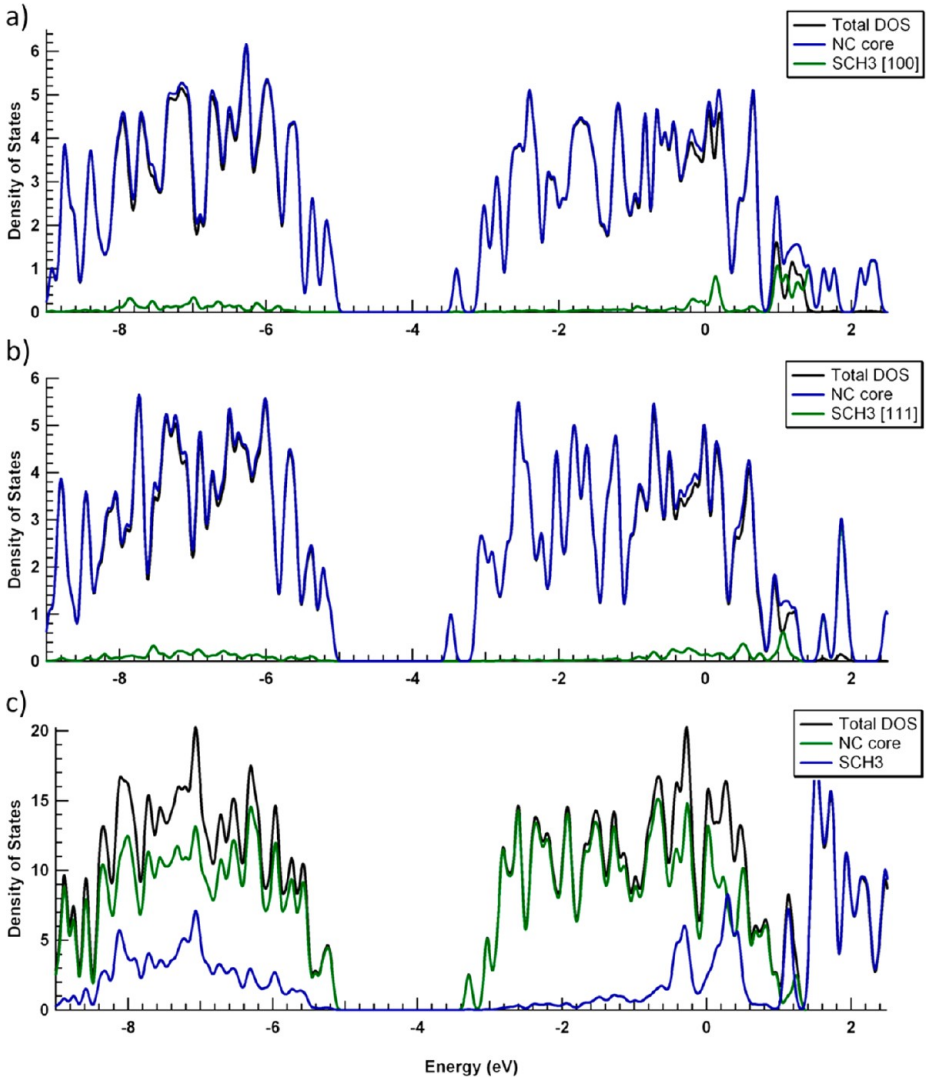

Figure 2. Projected density of states of a NC covered in ligands on some or all of the facets: (a) NC with -SCH_3^- ligands covering the [100] facets; (b) NC with SCH_3^- ligands covering the [111] facets; (c) NC with $-SCH_3^-$ ligands covering all facets. A 100 meV Gaussian broadening of peaks has been used.

not expected to contribute to optical transitions near the HOMO−LUMO gap energy, which arise primarily from the overlap of these wave functions. Ligand contributions can be seen high in the conduction orbitals (∼2 eV) in Figure 2a−c. In this higher energy state, the wave functions are localized over the ligand atoms and the NC core contribution is negligible. This can be clearly seen in Figure 3d where the isosurface (isovalue = 0.003) is shown for the orbital with primary contribution from the ligands. Overlap of these state wave functions with the HOMO is negligible and optical transitions into these states are expected to have a negligible transition matrix element. Hence, optical transitions just above the gap energy are expected primarily from orbitals localized on atoms in the NC core; ligand atoms should not contribute to the strong visible excitations.

Electronic Coupling. In this section, we calculate the electronic coupling of the NCs in four targeted studies that systematically target the effect of nanocrystal size, shape, and the presence of passivating ligands: 1.53 nm bare octahedral, ligand-clad octahedral, bare cube-octahedral, and 2.1 nm bare octahedral NCs. The coupling, or transfer integral, determines how strongly the wave functions of the energy levels of the adjacent NCs interact with each other, as defined in the Supporting Information. This property is directly proportional to the mobility of the system and hence its estimation is sufficient to provide a fundamental understanding of the charge transport in these model systems. For the one physical system in the set of four, namely, the ligand-passivated nanocrystals, we provide calculations of the mobility in a section that follows.

All the calculations in this section were carried out using the wB97X functional with the split basis sets of LANL2DZ/6-31+G(d,p). Two sets of coupling calculations were performed: (1) with [100] facets of the NCs

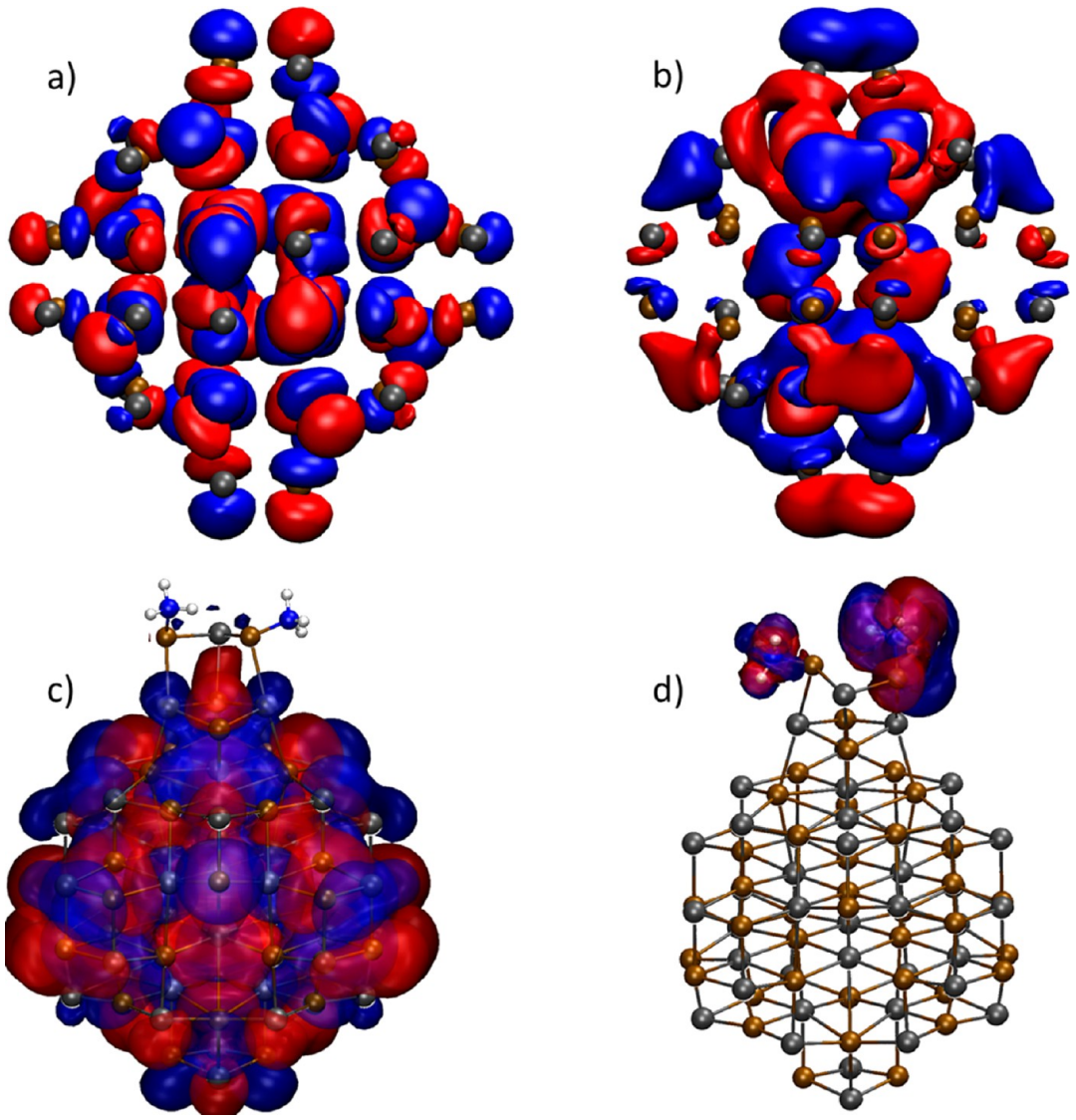

Figure 3. Orbital diagrams of the NC: (a) HOMO of the bare octahedral NC; (b) LUMO of the bare NC; (c) HOMO of the ligand-clad NC. (d) Orbital with strong contribution from the ligands (orbital energy ~2 eV). The goldenrod-colored spheres correspond to Se and the gray spheres to Pb atoms.

aligned and (2) with [111] facets aligned, as shown in Figure S4. Two NCs were initially placed 0.35 nm apart and then moved away from each other in steps of 0.1 nm. A single point calculation was performed at each step. This allowed us to determine the electron and hole coupling as a function of distance. We have not considered band-like charge transport which was found only for strongly coupled NCs,[50,51] as our systems lack conducting spacers. Moreover, Hyun *et al.* have shown that the charge transfer between NCs distant by thiol ligands is through nonadiabatic reaction.[52]

A 1.5 nm Bare NC. Coupling along the [100] direction for the 1.53 nm bare NC is shown as a function of distance in Figure 4. The coupling falls exponentially with distance in all the results presented here and can thus be fitted to a simple equation of the form $f(x) = a \exp(-bx)$, as shown in Figure 4. Semi-log plots of the electron and hole coupling along [100] and [111] facets are shown in Figure 5. Note that the distances involved are very small: all lie within a range of 0.5−0.7 nm. In experimental systems, NCs within the superlattice do not get closer than about 1.0 nm even for very short ligands.

Se atoms contribute toward hole coupling since the HOMO is centered on the Se atoms. Pb atoms contribute to the electron coupling since the LUMO is centered on the Pb atoms. The octahedral shape of the NC makes the HOMO wave function stretch along the [111] directions (since there are more Se atoms along the [111] direction). However, the Se atoms are located below the Pb atoms, further away. This makes the LUMO wave function spread in a complementary way to the HOMO. The spreading of the LUMO wave function is stronger along the [100] directions and weaker along the [111] directions; see Figure 3a,b.

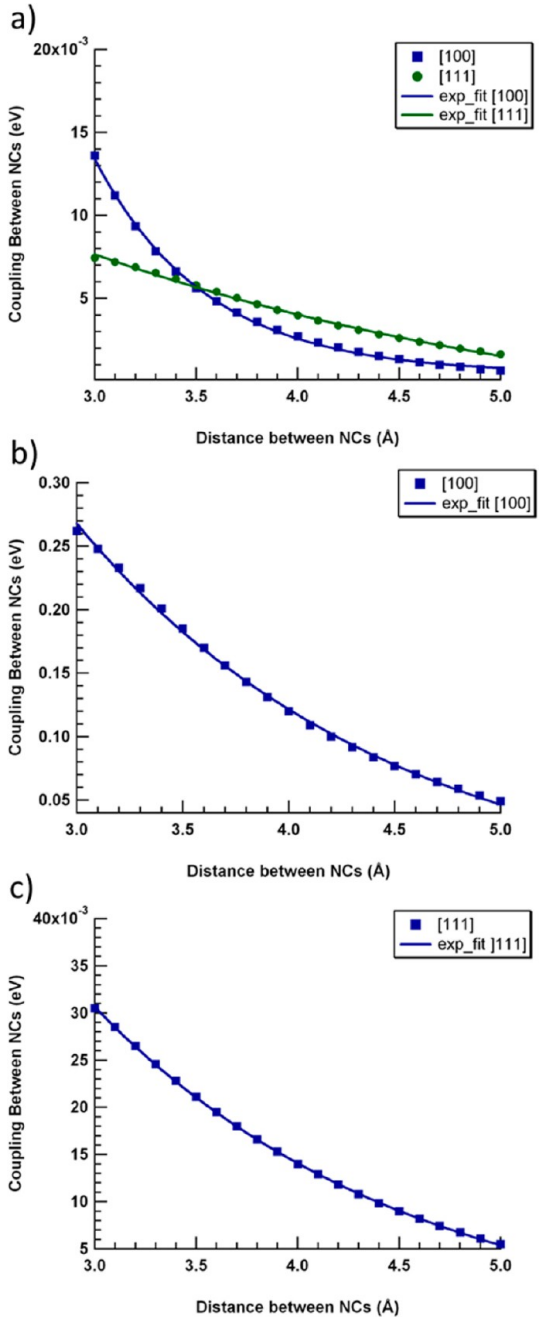

Figure 4. Coupling between the two bare NCs as a function of distance between the two: (a) hole coupling along the [100] and [111] directions; (b) electron coupling along [100]; (c) electron coupling along [111]. Symbols show calculated data. The solid line shows an exponential fit, as described in the text.

Electron coupling comes from overlap of the LUMO wave functions, and hole coupling from overlap of the HOMO wave functions. Thus, as seen in Figure 5, electron coupling is stronger along the [100] directions and weaker along the [111] directions, while the inverse is true for hole coupling. For the bare NC, electron coupling is stronger than hole coupling. This tends to make the charge reside within the NC core, and thus, the HOMO wave function does not "spill out"

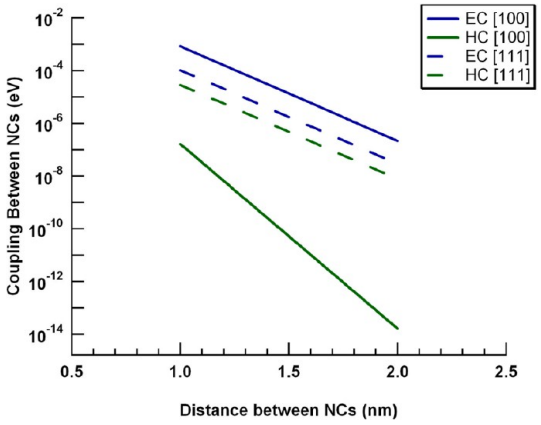

Figure 5. Semi-log plot of the coupling between bare NCs. EC, electron coupling (blue lines); HC, hole coupling (green lines). Coupling along [100] and [111] directions are shown as solid and dashed lines, respectively.

of the NC core as much as the LUMO. This makes hole coupling weaker than electron coupling (Figure 5).

The [100] facet has an alternating arrangement of Pb and Se atoms due to its rock salt lattice structure. Thus, if one NC is displaced along the [100] direction from the other NC, the Pb atom on the first NC aligns with the Se atom on the second, and the Se atom on the first NC aligns with the Pb atom on the second, as shown in Figure 6a. The total wave function of the NC along the [100] direction is the convolution of the wave functions due to the Pb and the Se atoms on the surface.

The HOMO is localized over the Se atoms so there is no charge density over the Pb atoms. The importance of this observation is that aligning Pb and Se atoms reduces coupling of the wave functions due to less interaction between wave functions over the Se atoms. If, on the other hand, the second NC is rotated by 90° with respect to the first, the Pb atoms (and the Se atoms) on both NCs would be aligned, as shown in Figure 6b. This leads to enhanced coupling. We conducted a series of simulations in which we rotated the second NC with respect to the first, in steps of 10°. The NCs were held at a constant separation of 0.5 nm. The results in Figure 7a,b show the variation of the electron and hole coupling as a function of the rotation angle, φ. The electron/hole coupling depends on whether the LUMO/HOMO wave function is positive or negative along the [100] direction. We find that the hole coupling decreases with an increase in φ, passes through zero and becomes negative. The zero crossing point occurs somewhere between 50° and 60°. At this point, the positive and negative components exactly offset one another, leading to completely decoupled HOMO levels for the dimer. A similar curve can also be seen in the electron coupling (Figure 7b), where the electron coupling becomes stronger (more negative) when the NCs are rotated by 90° with respect to each other.

It would be natural at this point to think that the exact angular orientation of the NCs would be

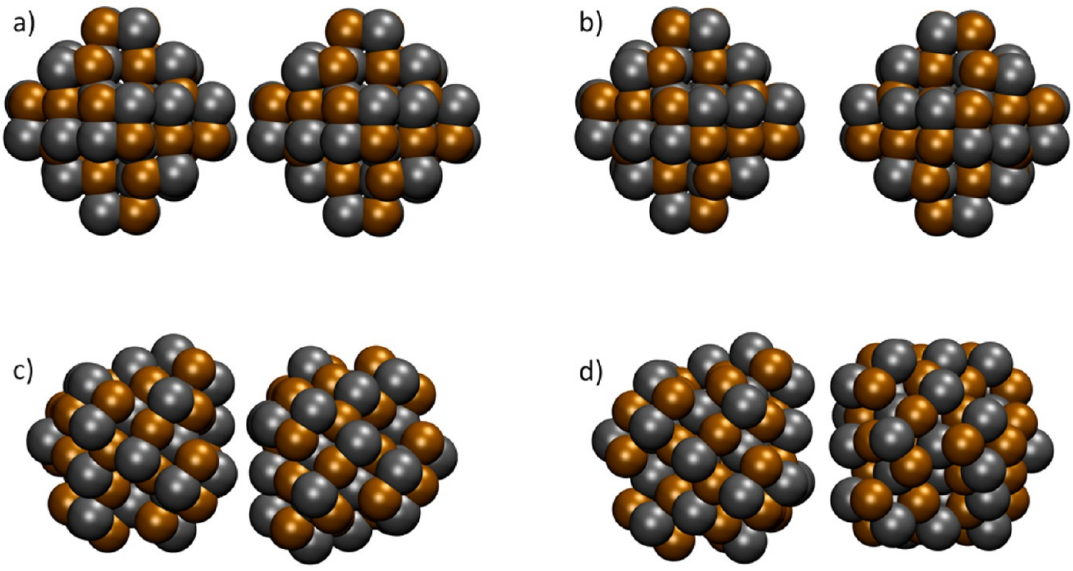

Figure 6. Two NCs aligned for coupling: (a) Pb and Se atoms on adjacent NCs aligned along the [100] direction, corresponding to 0°; (b) Pb−Pb and Se−Se atoms aligned along the [100] direction (90°); (c) NCs with triangular [111] facets orientationally displaced by 30°; (d) NCs with [111] facets orientationally aligned.

determined by the minimum energy interaction between the NCs. However, in order for the energetics of the NC cores to play a role, the NCs would need to be very close to each other and be devoid of ligands. This would not happen in a typical colloidal system where the NC cores are invariably covered by long chain alkyl ligands. If ligands filled the inter-NC region, the coupling would be quite different. Indeed, on the basis of Figure 3, there would be no HOMO−LUMO coupling in this case. In experimental systems, the orientation of the NC cores would be determined largely by the ligand interactions and one would generally encounter an ensemble average of orientations in a superlattice. Note that it is possible to observe aligned cores in a bcc superlattice using toluene as a solvent.[49,53] Accordingly, charge mobility in the superlattice represents an ensemble average of contributions arising from different orientations of the NC cores.

A similar set of simulations was performed for alignment along the [111] directions as shown in Figure 6c,d. For the triangular [111] facets, rotation by 120° returns the NC to its original orientation. The resulting hole coupling is shown in Figure 7c, where the initial orientation was such that triangular facets of adjacent NCs were staggered. Hole coupling is strongest when the triangular facets are staggered (0°) and weakest when the facets are completely eclipsed (60°). In cases where [111] facets of the NCs were orientationally aligned, i.e., in a bcc lattice,[49] hole coupling would be stronger than in an fcc lattice where the NCs are orientationally disordered.

A 2.1 nm Octahedral Bare NC: Examining the Effect of Size (Changing the Ratio of [100]:[111] Facet Areas). The NC considered in the previous section is an octahedron in which the ratio of [100] to [111] facet areas is about 0.3. To investigate our hypothesis that the spatial orientation of the HOMO/LUMO is based on the *relative areas* of [100] and [111] facets (as discussed in the previous section) and to investigate the effect of the ratio of area of facets, we simulated a larger, 2.1 nm, octahedral NC. This NC has the same [100] facet area as the 1.5 nm NC studied above, but has larger [111] facets. If our earlier hypothesis is correct, the HOMO coupling of this NC should again be much greater along the [111] direction than the [100] direction, as for the 1.5 nm NC.

Figure 8a shows that HOMO coupling along the [111] direction is indeed greater than along the [100] direction for two 2.1 nm NCs. The HOMO is oriented more along the [111] than [100] facets due to the former's larger facets. This provides evidence that keeping the [100] facet area the same and increasing the [111] facet area does not change the spatial orientation of the HOMO wave function. The LUMO spreads along the [100] directions, and hence, electron coupling along the [100] facets is greater than along [111] facets.

Figure 8b,c shows the comparison of electron and hole coupling between the 2.1 and 1.5 nm NCs. Both electron and hole coupling of the 2.1 nm NC are weaker than the 1.5 nm NC. Not surprisingly, smaller NCs produce stronger couplings, at least at very close distances. The decay of the electron coupling along the[100] direction is faster for smaller NCs, while it decays equally along the [111] direction (Figure 8b). Hole coupling decays faster for larger NCs (Figure 8c). But, as can be seen in Figure 8c, hole coupling of the 2.1 nm NC along the [111] direction has become stronger than that of the 1.5 nm NC along the [100] direction. This is clearly the effect of increasing the [111] facet area in the 2.1 nm NC. The HOMO is more

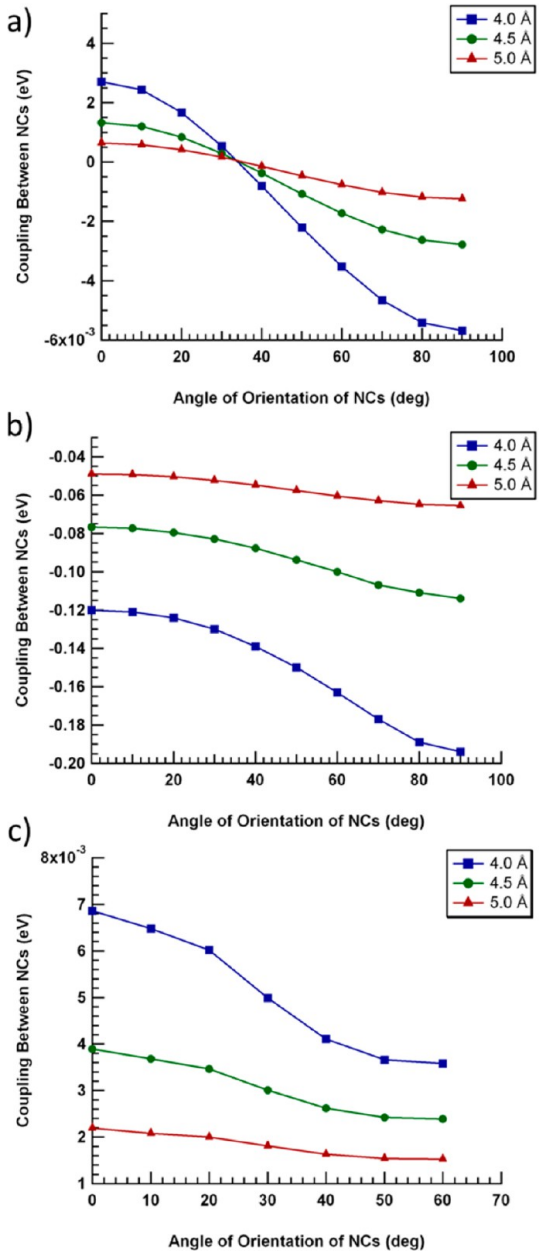

Figure 7. Electron and hole coupling of bare NCs at different distances as a function of angle of orientation: 0° corresponds to alternating Pb and Se atoms and 90° corresponds to an orientation in which Pb−Pb and Se−Se atoms are adjacent to each other. (a) Hole coupling along [100]. (b) Electron coupling along [100]. (c) Hole coupling along the [111] direction.

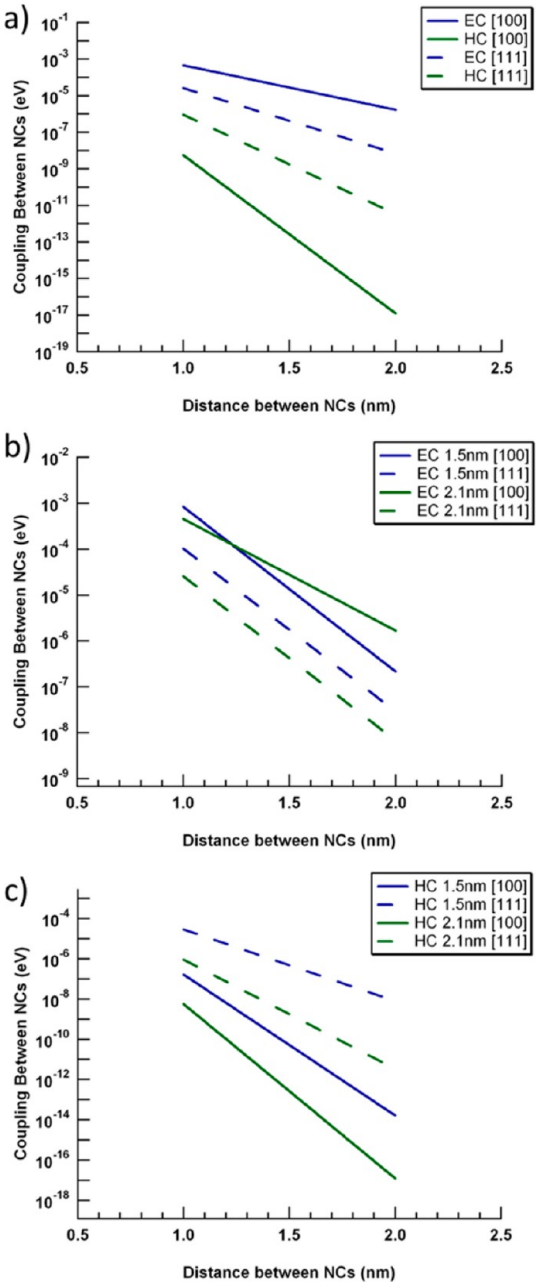

Figure 8. Coupling between bare 2.1 nm octahedral NCs: (a) electron and hole coupling along [100] and [111]; (b) comparison of electron coupling between 1.5 nm and 2.1 nm octahedral NCs; (c) similar comparison for the hole coupling.

orientationally aligned along the [111] facets in the larger NC since the [111] facet area is now larger. Consequently, the LUMO is more oriented along the [100] facets and the electron coupling of the 2.1 nm NC along the [100] direction is stronger than that of the smaller NC, as seen in Figure 8b. This is a clear indication that the facet area of the NC has an effect on the spatial orientation of the HOMO and LUMO wave functions and, consequently, on electron and hole coupling.

A 1.5 nm Cube-Octahedral Bare NC: Examining the Effect of Shape (Inverting the Ratio of [100]:[111] Facet Areas). The NCs considered in the previous sections have octahedral shapes and we looked at the effect of changing the area of the [111] facet. [In an octahedron, the area of the [111] facets is larger than that of the [100] facets, and there are more Pb atoms on the [111] facets.] In this section, we examine the effect of increasing the area of the [100] facets by calculating the electronic coupling of a 1.5 nm *cube-octahedral* NC. The 1.5 nm cube-octahedral NC has the same [111] facet area compared to 1.5 nm octahedral NC, but has a larger [100] facet area. The ratio of areas of [100] to

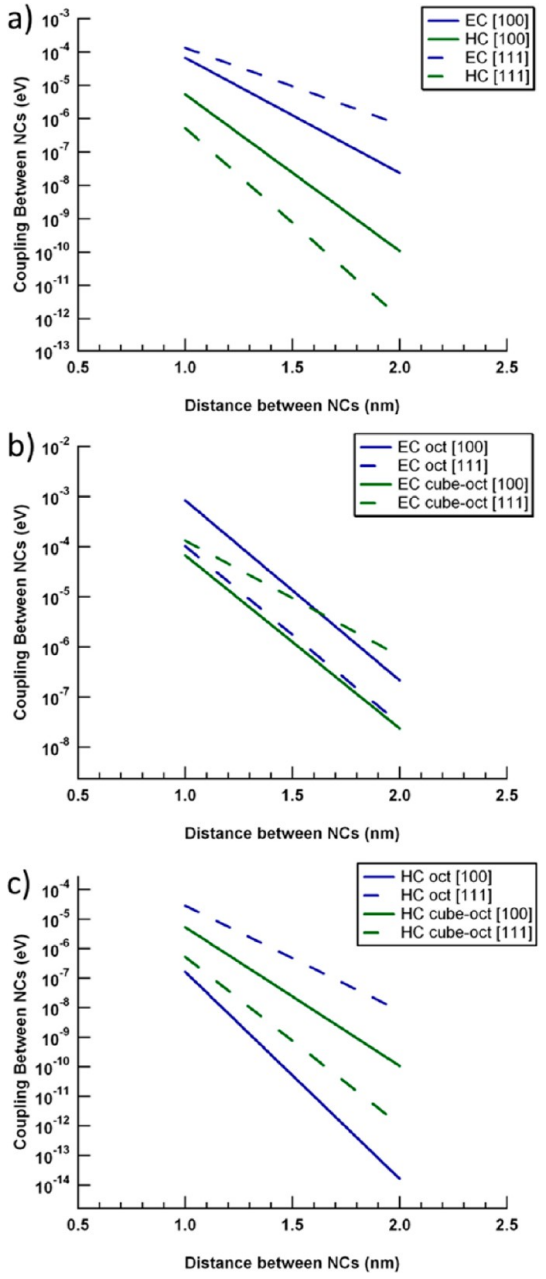

Figure 9. Coupling between bare cube-octahedral NCs: (a) electron and hole coupling along [100] and [111]; (b) comparison of electron coupling between octahedral and cube-octahedral NCs; (c) same comparison for hole coupling.

[111] facets is thus about 3.3 for the cube-octahedron (the inverse of the ratio of areas for the studies in previous sections).

Figure 9a shows electron and hole coupling of the cube-octahedral NC along the [100] and [111] directions. Electron coupling along the [111] direction is now stronger than along the [100] direction; hole coupling along the [100] direction has become larger than along [111]. The increase in [100] facet area for this shape of NC increases the number of Se atoms. This makes the HOMO wave function "bulge" more in the [100] direction, pushing the LUMO wave function away from the [100] facets and toward the [111] facets. Importantly, this is not simply an effect of size or the number of atoms in the NC. It is an effect arising from the *shape* of the NC and the (related) ratio of [100] to [111] facet areas, which gives directionality to the spatial orientation of the HOMO and LUMO wave functions. Electron coupling is, thus, weaker along the [100] direction than the [111] and *vice versa* for hole coupling.

Figure 9b,c shows a comparison of electron and hole coupling between octahedral and cube-octahedral NCs. Electron coupling along the [100] direction for the latter shape has decreased, and concomitantly increased along the [111] direction, as compared to the octahedral shape. The inverse is true for hole coupling. Thus, increasing the [100] facet area of the NC changes the spatial orientations of the HOMO and LUMO wave functions.

The importance of this finding will come into play for larger NCs. Experimental PbSe nanocrystals undergo a shape evolution from quasi-spherical to cube-octahedra to cubic with increasing nanocrystal size.[54,55] As the NC diameter increases, the area of the [111] facets shrinks and large NCs (~12−15 nm diameter) are almost cubic in shape with almost no significant [111] facets at all.

A 1.5 nm Ligand-Clad NC: Effect of Ligands. Colloidal NCs studied in a solution-processed experimental system are not bare; their surface is passivated by ligands. To study the effect of ligands, we used the method described in the Supporting Information to "cap" the NCs with HS^- ligands to provide surface passivation, as shown in Figure S5. For computational efficiency, we used the tiny HS^- ligand, to match the growing experimental trend and for computational efficacy. Short ligands promote closely spaced NC superlattices and hence improved coupling. We calculated the coupling between two NCs using the same methods described in previous sections.

Figure 10 shows the electron and hole couplings of ligand-clad NCs. One of the first observations is that hole coupling has become much stronger along both [100] and [111] facets. Now that the NC is no longer bare, the HOMO wave function can spread outside the NC, aided by the presence of the ligands. The slope of the hole coupling along the [111] direction decreases much more gradually with distance than those for bare NCs. On [100] facets, ligands sit on top of the Se atoms, where they block electron transfer and aid hole transfer. Consequently, as shown in Figure 10a, hole transfer curves increase in magnitude and become comparable to those for electron transfer.

Figure 10b shows a comparison of electron coupling between the bare and ligand-clad NCs. The effect of the ligands is to decrease electron coupling along the [100] direction. Electron transfer along the [100] and [111] directions is large at small distances (less than 1 and 1.5 nm, respectively) because ligands on the

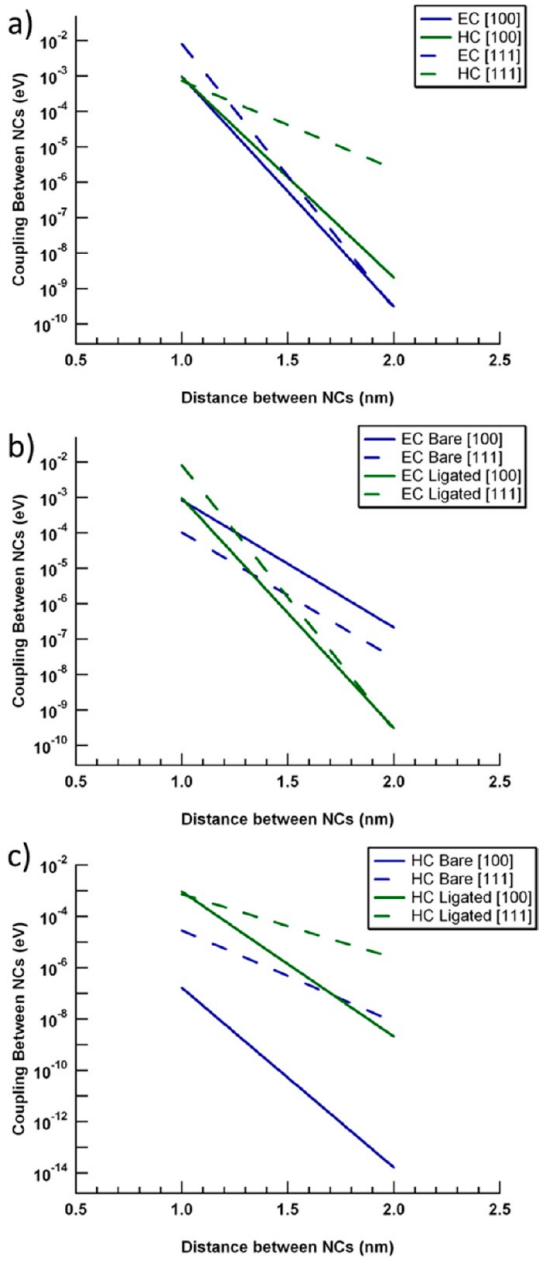

Figure 10. Coupling between ligand-clad NCs: (a) electron and hole coupling along [100] and [111] directions; (b) comparison of electron coupling between bare and ligand-clad NCs; (c) similar comparison for the hole coupling.

facets on adjacent NCs are very close to each other, and thus, there is some electronic coupling between the ligands themselves. This is manifested as electron coupling between the NCs. But the electron coupling has a steep slope and falls off very quickly as the distance increases in systems containing ligands as compared to bare NCs. In contrast, ligands greatly enhanced hole transport (Figure 10c).

We computed the reorganization energy as described in section S1.2 in the Supporting Information, and then computed electron and hole transfer rates as described in section S1. The resulting curves of charge transfer rate as a function of distance between NCs are

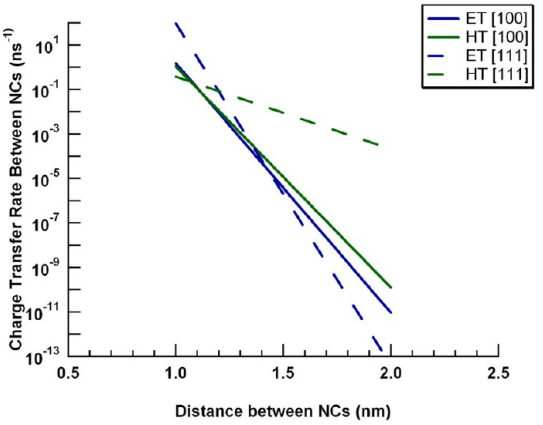

Figure 11. Charge transfer rates between ligand-clad NCs. Electron and hole transfer rates are shown along the [100] and [111] directions.

shown in Figure 11. The reorganization energies are proportional to the square of the electron and hole coupling values, as described in section S1. The electron/hole transfer rates found here occur on the order of nanoseconds. As seen in Figure 11, the time scale for hole transport along the [111] direction over a distance of 1−2 nm ranges from 10 to 100 ns. Experimentally determined rates for NC systems do exist, affording a comparison: At a separation of 1.5 nm, the experimentally computed transfer rate for a larger 2.7 nm diameter PbS NC is about 0.5−1.0 ns.[53]

Choi *et al.* report a rate of decay of the charge transfer curve to be about 2.6;[56] our decay rates for the data shown in Figure 11 range from 0.75 to 3.5. Thus, the range of our decay rates encompasses the experimentally fitted one. There may be several reasons for the factor of 50−100 difference in the absolute magnitude of the transfer rates. The presence of solvents (not feasible in these calculations), for instance, can dramatically affect charge transfer rates depending on the dielectric constant of the solvent.[57] For instance, Hyun *et al.* find that changing the solvent from an organic molecule to water can increase charge transfer rates by a factor of 1000.[52] The chemical nature (polarity) of the solvent could propagate (or screen) the charges on the NCs and hence increase (or decrease) charge transfer between the NCs. Decreasing the size of the NCs from the experimental value of 2.7 nm[56] to the simulation's 1.5 nm will also have an effect. Using Liu *et al.*'s experimental data for the dependence of mobility on NC diameter will easily cause a decrease in mobility by at least an order of magnitude.[58] Given these comparisons, our values appear to be very similar to those that might be obtained experimentally if it were possible to fabricate a system of tightly size-controlled 1.5 nm PbSe NCs without any solvent present. Changing the basis set, *e.g.*, from LANL2DZ to LANL2DZdp, did not significantly affect the results.

Charge Carrier Mobility. We computed the electron and hole mobilities for the 1.5 nm octahedral ligand-clad NC,

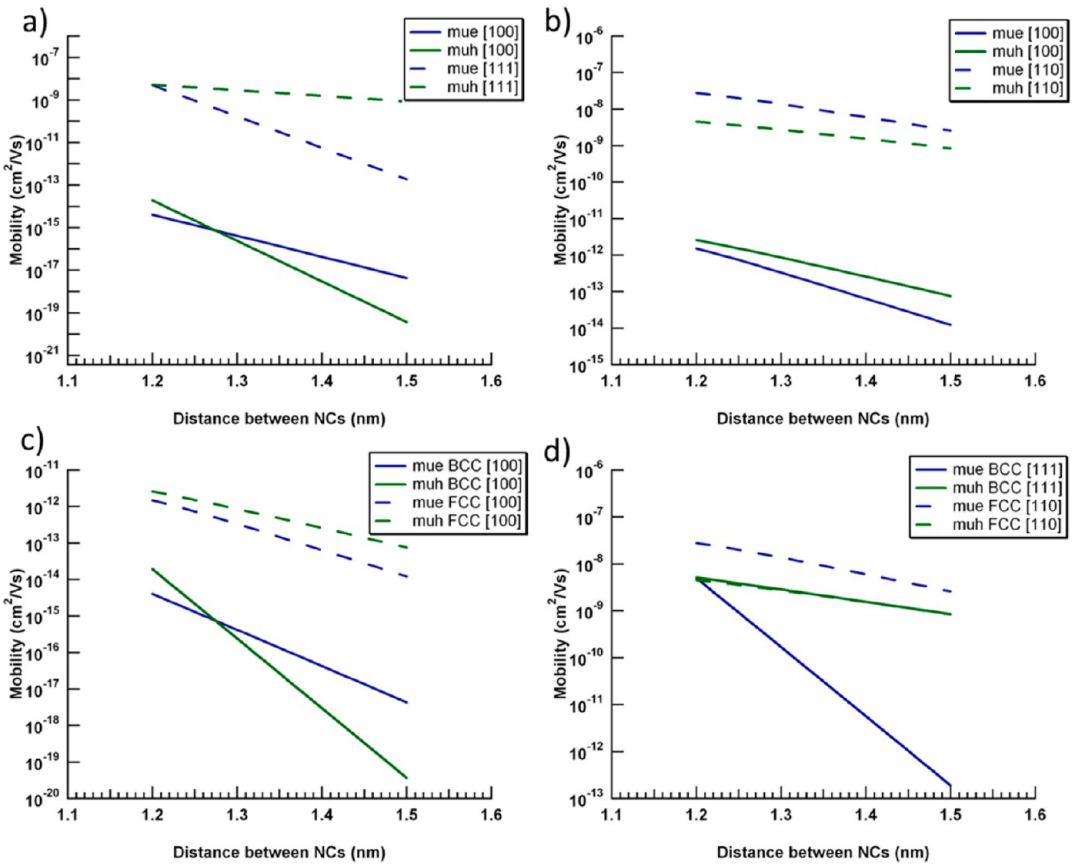

Figure 12. (a and b) Mobility in bcc and fcc superlattices, respectively, as a function of nearest neighbor (NN) distance. (c) Comparison of mobilities along the [100] direction in bcc and fcc lattices. (d) A similar comparison along the NN directions in bcc (111) and fcc (110) lattices. Key: Electron mobilities in blue, hole mobilities in green. Hole and electron mobilities listed as mu(h) and mu(e), respectively, in the insets.

as described above, for bcc and fcc superlattices along the [100] (2nd NN) direction, and along the nearest neighbor (NN) directions, *i.e.*, [111] in bcc and [110] in fcc. These high-symmetry directions are essentially special cases of the random hopping between neighbors in the lattice. The mobility was computed using the charge transfer rates between NCs with ligands from previous section and is shown in Figure 12. All possible neighbors at the corresponding distances were considered when calculating the relative probability of the charge hopping in a certain direction.

The nearest neighbor (NN) distance along the [100] direction will be $2d/\sqrt{3}$ for bcc and $\sqrt{2}d$ for fcc. As seen in Figure 12a,b, both the electron and hole mobilities along the NN direction are 4−6 orders of magnitude greater than along the 2NN [100] direction. In a bcc lattice, the NCs are known experimentally to be orientationally ordered[53] and [100] and [111] facets are aligned. Mobility along [100] direction is much high in fcc superlattice compared to bcc (Figure 12c). The hole mobility is greater than the electron mobility along the [111] direction, and the electron mobility decays much faster than the hole mobility along the [111] direction (Figure 12d). In the fcc lattice, however, the NCs are orientationally disordered and this results in a random mix of alignment between [100]−[100], [100]−[111] and [111]−[111] facets. The mobility along any direction will thus be the weighted average of all the rates of charge transfer noted above. This results in the electron and hole mobilities being comparable along [100] and [111] directions. Comparing bcc and fcc lattices, we can see that, as the NN distance between the NCs increases, both the electron and hole mobilities along the [100] direction are higher in an fcc lattice than a bcc lattice (Figure 12a). Along the NN direction, electron mobility in the bcc lattice is very low and falls off steeply with distance since the electron transfer rate between the [111] facets is very small. Hole mobility in the bcc lattice and electron and hole mobility in the fcc lattice are comparable.

Thus, the highest mobility depends on the type of lattice as well as the direction along which the mobility is measured which, in turn, is governed by the shape of the NCs and the ratio of areas of the [100] and [111] facets. In general, if it were possible to choose between a bcc and an fcc lattice symmetry, but the NCs displayed large [111] facets, either a bcc or an fcc lattice symmetry would be desirable. In contrast, if the NCs exhibited large [100] facets, an fcc lattice symmetry would be much more desirable than a bcc lattice symmetry.

From Figure 12, we can see that our calculated electron and hole mobilities are on the order of 10^{-7} to 10^{-15} cm^2 V^{-1} s^{-1} at a distance of about 1.2 nm, as dictated by the presence of the ligands, and depending on the orientation of the NCs. These mobilities are, of course, very small and comparison to known experimental values of the mobilities of PbSe NCs is tempting. We will discuss such a comparison in detail in the Conclusions section.

CONCLUSIONS

We have presented calculations of the electronic structure and charge transport characteristics of PbSe NC systems using DFT without the need to employ any particular approximations or combinations of approaches. We have calculated the structure of the bare NCs and shown how reconstruction of the surface can lower the energy of the NC (Supporting Information). [110] facets, alluded to exist in ref 30, are not considered here. If they exist, they are likely to be very small in comparison to [100] and [111] facets and will only appear in larger NCs than we have considered. We have used a method of ligand attachment (Supporting Information) that, importantly, ensures charge neutrality of the whole NC based on the technique developed by Bealing *et al.*[30] The surface reconstruction and ligand attachment considered here are such that all possible atomic sites are filled. In real systems, facet reconstruction may not be perfect and all possible sites may not be occupied by ligands. A random arrangement of reconstructed atomic sites and ligand arrangement could alter the envelope of the wave functions and would be an interesting problem for a future systematic study. We have not considered dispersion forces between the ligand molecules, but they would need to be taken into account if a larger NC were considered with longer chain ligands since they dictate how densely the ligands could be grafted onto the facets.[30]

Our key findings are, first, that the density of states of the bare NC are nearly symmetric, providing computational confirmation of Overgaag's experimental data.[26] The DOS for both bare and SCH_3^- ligand-clad NCs show that the filled states are centered around the Se atoms and unfilled states around the Pb atoms. The ligand states are well mixed with the core atoms and do not contribute greatly toward the frontier orbitals. We also showed that a delta peak that appears as an isolated state from the conduction band in octahedral NCs does not arise from a localized trap.

Importantly, we have shown conclusively that the spatial orientation of the wave function depends on the *shape* of the NC and the *relative areas of [100] and [111] facets*. This delineates precisely how shape affects charge transport characteristics in small nanocrystals. The larger the facet area, the more the HOMO is oriented along that direction, which makes the LUMO spread in the complementary direction. We have shown that orientational alignment of the NC itself can significantly affect coupling and charge transfer. The orientation of the HOMO and LUMO determines how much overlap occurs along a particular direction and, thus, determines the strength of the coupling. In this regard, an octahedral shape showed strong electron coupling along the [100] direction and strong hole coupling along the [111] direction, whereas a cube-octahedral shape showed strong electron coupling along the [111] direction and strong hole coupling along the [100] direction.

Our studies of the effect of ligands on electronic coupling show that the type of short ligands considered here *enhance hole* coupling and *shield electron* coupling. There have been complementary experimental studies where the NCs have been treated to enhance *electron* coupling; for example, PbSe NCs treated with hydrazine showed reversible transitions from n-type to p-type.[15] Thus, appropriate ligand chemistry can be utilized to produce both electron and hole transfer in these NC systems and can provide a gateway to produce ambipolar devices. Some NC systems are known to exhibit anisotropic ligand coverage,[30] typically due to loss of ligand coverage. For example, NCs exposed to air for a long time have been hypothesized to lose ligands preferentially from [100] facets[59] and reassemble into orientationally aligned bcc superlattices. This would lead to large hole transport along the [111] directions. Such asymmetric ligand grafting could lead to enhanced charge transfer along certain preferred directions. If ligand attachment could be controlled, which is not currently achievable experimentally, it would be possible, in principle, to create self-assembled superlattices with an appropriate symmetry to produce the greatest possible charge transfer characteristics.

We have also calculated the charge mobility in bcc and fcc superlattices. We determined a range of rates of decay of the charge transfer curve that encompasses the experimentally fitted one[59] in roughly the middle of the range we predict. The absolute charge transfer rates calculated here are a factor of about 100 smaller than those of experimental systems.[58] Comparison to experimental mobilities is also instructive. For 8 nm-diameter PbSe NCs, values of the mobility as high as ~1.0 cm^2 V^{-1} s^{-1} can be achieved after chemical treatment with hydrazine.[15] However, NC size has a significant influence on mobility, as shown by Liu *et al.*[58] They see that mobility decreases quickly as the size of the NC decreases. For example, the electron mobility drops to 6×10^{-3} cm^2 V^{-1} s^{-1} for 3.1 nm-diameter NCs.[58] If we extrapolate Liu *et al.*'s values to our 1.53 nm-diameter NCs, we should expect mobilities on the order of 10^{-4} cm^2 V^{-1} s^{-1} for electrons and 10^{-5} cm^2 V^{-1} s^{-1} for holes.

A second mediating factor arises from the fact that we have calculated mobilities at separations no shorter

than 1.2−1.5 nm that are consistent with the length of ligands typically used for colloidal nanocrystals (1.5 nm) and the closest separation that they typically achieve by interdigitation (∼1.2 nm). Liu *et al.* have shown an inverse relationship between ligand length (which is related to the inter-NC distance; not given) and mobility.[58] An order of magnitude decrease in mobility was measured for an increase in ligand length by 2.5 Å. Talapin and Murray have also shown increase in mobility with the usage of shorter ligands.[15] Since mobility decreases with increased separation, this can be expected to lead to lower mobilities

Finally, a third factor that will affect the mobility concerns the role of the solvent, which we are not able to include here due to the computational expense. Charge transfer rates certainly depend on the type of solvent used (polar or nonpolar). Hyun *et al.* have shown that charge transfer rates can increase by up to 1000 times as the dielectric constant of the solvent increases.[52] We can therefore safely assume that solvents contribute to the increased mobility in experiments.

Consideration of each of these three factors improves the comparison of our results with experiment. Summing the likely contributions above suggests that the numerical value of our mobilities is not far from what would be achieved by identical experiments.

Clearly, more effective charge transfer occurs if the NCs can approach closely (∼1 nm). This is consistent with the improvement in transport observed experimentally using compact linker molecules such as ethane di-thiol (EDT), pyrazine, hydrazine, benzene di-thiol (BDT), *etc.*[11,15,25−28] But the use of linker molecules does not come without drawbacks. Since these molecules link NCs together through chemical bonds, the NCs lose some of their quantum confinement and can result in disordered superlattices.[11,56] Nevertheless, they form an interesting study, and we hope that the study presented here will encourage others to model, and perhaps screen for optimal performance, systems of NCs linked through candidate small molecules.

METHODS

We have used Marcus theory to calculate charge transfer; since this is a standard technique, we have relegated the details to the Supporting Information. Details of our use of Gaussian09[60] and the procedure used to optimize the structures of the bare NCs are also discussed in the Supporting Information. The Supporting Information also describes the method used to graft ligands onto the surface of the NCs; this is a critical piece of the method and has to be carried out with great precision.

Once we had obtained optimized (energy-minimized) structures of both bare and ligand-clad NCs using Gaussian09, as described in the Supporting Information, we performed single point energy calculations using the Gaussian09-supplied HSEh1PBE functional in conjunction with the LANL2DZ basis set for the bare NC, and the split LANL2DZ/6-31+G(d,p) basis set for the ligand-clad NC. We also performed electronic coupling simulations of the NC dimers by placing the NCs at different distances from each other along [100] and [111] directions. The wB97X functional was used for these calculations since it has been found to perform well in previous studies to calculate coupling.[61] The NCs were rotated appropriately so that their [100] and [111] facets were aligned for these calculations. A similar procedure was used for the 1.53 nm cube-octahedron NC, although for this shape of NC only the bare reconstructed structures were used.

Conflict of Interest: The authors declare no competing financial interest.

Acknowledgment. This publication was based on work supported by Award No. KUS-C1-018-02, made by the King Abdullah University of Science and Technology (KAUST). Intel Corporation is thanked for the donation of computing resources crucial to the studies performed here. Thibault Cremel, a Master's student in Fundamental Physics and Nanosciences at the University Joseph Fourier in Grenoble, is thanked for his sterling contributions to this study during a summer study visit to Cornell. Cornell colleagues, Professors Frank Wise, Richard Hennig, Tobias Hanrath and Nandini Ananth are thanked for reading the manuscript and for their helpful suggestions for improvement.

Supporting Information Available: Description of the theory used, details of simulation, projected density of states of octahedral NCs and details and figures of NCs and their alignment. This material is available free of charge *via* the Internet at http://pubs.acs.org.

REFERENCES AND NOTES

1. Bhattacharya, P.; Ghosh, S.; Stiff-Roberts, A. D. Quantum Dot Opto-Electronic Devices. *Annu. Rev. Mater. Res.* **2004**, *34*, 1–40.
2. Law, M.; Goldberger, J.; Yang, P. D. Semiconductor Nanowires and Nanotubes. *Annu. Rev. Mater. Res.* **2004**, *34*, 83–122.
3. Skolnick, M. S.; Mowbray, D. J. Self-Assembled Semiconductor Quantum Dots: Fundamental Physics and Device a Tipplications. *Annu. Rev. Mater. Res.* **2004**, *34*, 181–218.
4. Murray, C. B.; Kagan, C. R.; Bawendi, M. G. Synthesis and Characterization of Monodisperse Nanocrystals and Close-Packed Nanocrystal Assemblies. *Annu. Rev. Mater. Sci.* **2000**, *30*, 545–610.
5. Talapin, D. V; Lee, J.-S.; Kovalenko, M. V; Shevchenko, E. V. Prospects of Colloidal Nanocrystals for Electronic and Optoelectronic Applications. *Chem. Rev.* **2010**, *110*, 389–458.
6. Alivisatos, A. P. Perspectives on the Physical Chemistry of Semiconductor Nanocrystals. *J. Phys. Chem.* **1996**, *100*, 13226–13239.
7. Wu, Y.; Wadia, C.; Ma, W.; Sadtler, B.; Alivisatos, A. P. Synthesis and Photovoltaic Application of Copper(I) Sulfide Nanocrystals. *Nano Lett.* **2008**, *8*, 2551–2555.
8. Panthani, M. G.; Akhavan, V.; Goodfellow, B.; Schmidtke, J. P.; Dunn, L.; Dodabalapur, A.; Barbara, P. F.; Korgel, B. A. Synthesis of $CuInS_2$, $CuInSe_2$, and $Cu(In_xGa_{1-x})Se_2$ (CIGS) Nanocrystal "Inks" for Printable Photovoltaics. *J. Am. Chem. Soc.* **2008**, *130*, 16770–16777.
9. Choi, J. J.; Lim, Y.-F.; Santiago-Berrios, M. B.; Oh, M.; Hyun, B.-R.; Sung, L.; Bartnik, A. C.; Goedhart, A.; Malliaras, G. G.; Abruna, H. D.; *et al.* PbSe Nanocrystal Excitonic Solar Cells. *Nano Lett.* **2009**, *9*, 3749–3755.
10. Ma, W.; Luther, J. M.; Zheng, H.; Wu, Y.; Alivisatos, A. P. Photovoltaic Devices Employing Ternary PbSxSe1-x Nanocrystals. *Nano Lett.* **2009**, *9*, 1699–1703.
11. Luther, J. M.; Law, M.; Beard, M. C.; Song, Q.; Reese, M. O.; Ellingson, R. J.; Nozik, A. J. Schottky Solar Cells Based on

Colloidal Nanocrystal Films. *Nano Lett.* **2008**, *8*, 3488–3492.
12. Leschkies, K. S.; Beatty, T. J.; Kang, M. S.; Norris, D. J.; Aydil, E. S. Solar Cells Based on Junctions Between Colloidal PbSe Nanocrystals and Thin ZnO Films. *ACS Nano* **2009**, *3*, 3638–3648.
13. Urban, J. J.; Talapin, D. V; Shevchenko, E. V; Kagan, C. R.; Murray, C. B. Synergism in Binary Nanocrystal Superlattices Leads to Enhanced p-Type Conductivity in Self-Assembled PbTe/Ag_2 Te Thin Films. *Nat. Mater.* **2007**, *6*, 115–121.
14. Sun, B.; Sirringhaus, H. Solution-Processed Zinc Oxide Field-Effect Transistors Based on Self-Assembly of Colloidal Nanorods. *Nano Lett.* **2005**, *5*, 2408–2413.
15. Talapin, D. V; Murray, C. B. PbSe Nanocrystal Solids for n- and p-Channel Thin Film Field-Effect Transistors. *Science* **2005**, *310*, 86–89.
16. Coe, S.; Woo, W. K.; Bawendi, M.; Bulovic, V. Electroluminescence from Single Monolayers of Nanocrystals in Molecular Organic Devices. *Nature* **2002**, *420*, 800–803.
17. Mueller, A. H.; Petruska, M. A.; Achermann, M.; Werder, D. J.; Akhadov, E. A.; Koleske, D. D.; Hoffbauer, M. A.; Klimov, V. I. Multicolor Light-Emitting Diodes Based on Semiconductor Nanocrystals Encapsulated in GaN Charge Injection Layers. *Nano Lett.* **2005**, *5*, 1039–1044.
18. McDonald, S. A.; Konstantatos, G.; Zhang, S. G.; Cyr, P. W.; Klem, E. J. D.; Levina, L.; Sargent, E. H. Solution-Processed PbS Quantum Dot Infrared Photodetectors and Photovoltaics. *Nat. Mater.* **2005**, *4*, 138–142.
19. Shipway, A. N.; Katz, E.; Willner, I. Nanoparticle Arrays on Surfaces for Electronic, Optical, and Sensor Applications. *ChemPhysChem* **2000**, *1*, 18–52.
20. Akhavan, V. A.; Goodfellow, B. W.; Panthani, M. G.; Reid, D. K.; Hellebusch, D. J.; Adachi, T.; Korgel, B. A. Spray-Deposited $CuInSe_2$ Nanocrystal Photovoltaics. *Energy Environ. Sci.* **2010**, *3*, 1600–1606.
21. Akhavan, V. A.; Goodfellow, B. W.; Panthani, M. G.; Korgel, B. A. Towards a Next Generation of Ultra-Low-Cost Photovoltaics Using Nanocrystal Inks. *Mod. Energy Rev.* **2010**, *2*, 25–27.
22. Murray, C. B.; Sun, S. H.; Gaschler, W.; Doyle, H.; Betley, T. A.; Kagan, C. R. Colloidal Synthesis of Nanocrystals and Nanocrystal Superlattices. *IBM J. Res. Dev.* **2001**, *45*, 47–56.
23. Liljeroth, P.; Overgaag, K.; Urbieta, A.; Grandider, B.; Hickey, S. G.; Vanmaekelbergh, D. Variable Orbital Coupling in a Two-Dimensional Quantum-Dot Solid Probed on a Local Scale. *Phys. Rev. Lett.* **2006**, *97*, 096803.
24. Lee, B.; Podsiadlo, P.; Rupich, S.; Talapin, D. V; Rajh, T.; Shevchenko, E. V. Comparison of Structural Behavior of Nanocrystals in Randomly Packed Films and Long-Range Ordered Superlattices by Time-Resolved Small Angle X-ray Scattering. *J. Am. Chem. Soc.* **2009**, *131*, 16386–16388.
25. Kovalenko, M. V; Scheele, M.; Talapin, D. V. Colloidal Nanocrystals with Molecular Metal Chalcogenide Surface Ligands. *Science* **2009**, *324*, 1417–1420.
26. Overgaag, K.; Liljeroth, P.; Grandidier, B.; Vanmaekelbergh, D. Scanning Tunneling Spectroscopy of Individual PbSe Quantum Dots and Molecular Aggregates Stabilized in an Inert Nanocrystal Matrix. *ACS Nano* **2008**, *2*, 600–606.
27. Koh, W.; Saudari, S. R.; Fafarman, A. T.; Kagan, C. R.; Murray, C. B. Thiocyanate-Capped PbS Nanocubes: Ambipolar Transport Enables Quantum Dot Based Circuits on a Flexible Substrate. *Nano Lett.* **2011**, *11*, 4764–4767.
28. Choi, J.-H.; Fafarman, A. T.; Oh, S. J.; Ko, D.-K.; Kim, D. K.; Diroll, B. T.; Muramoto, S.; Gillen, J. G.; Murray, C. B.; Kagan, C. R. Bandlike Transport in Strongly Coupled and Doped Quantum Dot Solids: A Route to High-Performance Thin-Film Electronics. *Nano Lett.* **2012**, *12*, 2631–2638.
29. Fang, C.; van Huis, M. A.; Vanmaekelbergh, D.; Zandbergen, H. W. Energetics of Polar and Nonpolar Facets of PbSe Nanocrystals from Theory and Experiment. *ACS Nano* **2010**, *4*, 211–218.
30. Bealing, C. R.; Baumgardner, W. J.; Choi, J. J.; Hanrath, T.; Hennig, R. G. Predicting Nanocrystal Shape through Consideration of Surface-Ligand Interactions. *ACS Nano* **2012**, *6*, 2118–2127.
31. Luo, J.-W.; Franceschetti, A.; Zunger, A. Carrier Multiplication in Semiconductor Nanocrystals: Theoretical Screening of Candidate Materials Based on Band-Structure Effects. *Nano Lett.* **2008**, *8*, 3174–3181.
32. Franceschetti, A.; Wang, L. W.; Bester, G.; Zunger, A. Confinement-Induced *versus* Correlation-Induced Electron Localization and Wave Function Entanglement in Semiconductor Nano Dumbbells. *Nano Lett.* **2006**, *6*, 1069–1074.
33. An, J. M.; Franceschetti, A.; Zunger, A. The Excitonic Exchange Splitting and Radiative Lifetime in PbSe Quantum Dots. *Nano Lett.* **2007**, *7*, 2129–2135.
34. An, J. M.; Franceschetti, A.; Dudiy, S. V; Zunger, A. The Peculiar Electronic Structure of PbSe Quantum Dots. *Nano Lett.* **2006**, *6*, 2728–2735.
35. Califano, M.; Bester, G.; Zunger, A. Prediction of a Shape-Induced Enhancement in the Hole Relaxation in Nanocrystals. *Nano Lett.* **2003**, *3*, 1197–1202.
36. Kiran, B.; Kandalam, A. K.; Rallabandi, R.; Koirala, P.; Li, X.; Tang, X.; Wang, Y.; Fairbrother, H.; Gantefoer, G.; Bowen, K. (PbS)(32): A Baby Crystal. *J. Chem. Phys.* **2012**, *136*, 024317.
37. Gai, Y.; Peng, H.; Li, J. Electronic Properties of Nonstoichiometric PbSe Quantum Dots from First Principles. *J. Phys. Chem. C* **2009**, *113*, 21506–21511.
38. Voznyy, O. Mobile Surface Traps in CdSe Nanocrystals with Carboxylic Acid Ligands. *J. Phys. Chem. C* **2011**, *115*, 15927–15932.
39. Fischer, S. A.; Crotty, A. M.; Kilina, S. V; Ivanov, S. A.; Tretiak, S. Passivating Ligand and Solvent Contributions to the Electronic Properties of Semiconductor Nanocrystals. *Nanoscale* **2012**, *4*, 904–914.
40. Bao, H.; Habenicht, B. F.; Prezhdo, O. V; Ruan, X. Temperature Dependence of Hot-Carrier Relaxation in PbSe Nanocrystals: An *ab Initio* Study. *Phys. Rev. B* **2009**, *79*, 235306.
41. Jaeger, H. M.; Fischer, S.; Prezhdo, O. V. The Role of Surface Defects in Multi-Exciton Generation of Lead Selenide and Silicon Semiconductor Quantum Dots. *J. Chem. Phys.* **2012**, *136*, 064701.
42. Chu, I.-H.; Radulaski, M.; Vukmirovic, N.; Cheng, H.-P.; Wang, L.-W. Charge Transport in a Quantum Dot Supercrystal. *J. Phys. Chem. C* **2011**, *115*, 21409–21415.
43. Franceschetti, A. Structural and Electronic Properties of PbSe Nanocrystals from First Principles. *Phys. Rev. B* **2008**, *78*, 075418.
44. Franceschetti, A. First-Principles Calculations of the Temperature Dependence of the Band Gap of Si Nanocrystals. *Phys. Rev. B* **2007**, *76*, 161301.
45. Kang, I.; Wise, F. W. Electronic Structure and Optical Properties of PbS and PbSe Quantum Dots. *J. Opt. Soc. Am. B* **1997**, *14*, 1632–1646.
46. Nootz, G.; Padilha, L. A.; Olszak, P. D.; Webster, S.; Hagan, D. J.; Van Stryland, E. W.; Levina, L.; Sukhovatkin, V.; Brzozowski, L.; Sargent, E. H. Role of Symmetry Breaking on the Optical Transitions in Lead-Salt Quantum Dots. *Nano Lett.* **2010**, *10*, 3577–3582.
47. Diaconescu, B.; Padilha, L. A.; Nagpal, P.; Swartzentruber, B. S.; Klimov, V. I. Measurement of Electronic States of PbS Nanocrystal Quantum Dots Using Scanning Tunneling Spectroscopy: The Role of Parity Selection Rules in Optical Absorption. *Phys. Rev. Lett.* **2013**, *110*, 127406.
48. Yu, M.; Fernando, G. W.; Li, R.; Papadimitrakopoulos, F.; Shi, N.; Ramprasad, R. First Principles Study of CdSe Quantum Dots: Stability, Surface Unsaturations, and Experimental Validation. *Appl. Phys. Lett.* **2006**, *88*, 231910.
49. Ip, A. H.; Thon, S. M.; Hoogland, S.; Voznyy, O.; Zhitomirsky, D.; Debnath, R.; Levina, L.; Rollny, L. R.; Carey, G. H.; Fischer, A.; *et al.* Hybrid Passivated Colloidal Quantum Dot Solids. *Nat. Nanotechnol.* **2012**, *7*, 577–582.
50. Lee, J.-S.; Kovalenko, M. V; Huang, J.; Chung, D. S.; Talapin, D. V. Band-Like Transport, High Electron Mobility and High Photoconductivity in All-Inorganic Nanocrystal Arrays. *Nat. Nanotechnol.* **2011**, *6*, 348–352.
51. Talgorn, E.; Gao, Y.; Aerts, M.; Kunneman, L. T.; Schins, J. M.; Savenije, T. J.; van Huis, M. A.; van der Zant, H. S. J.; Houtepen, A. J.; Siebbeles, L. D. A. Unity Quantum Yield

of Photogenerated Charges and Band-Like Transport in Quantum-Dot Solids. *Nat. Nanotechnol.* **2011**, *6*, 733–739.
52. Hyun, B.-R.; Bartnik, A. C.; Lee, J.-K.; Imoto, H.; Sun, L.; Choi, J. J.; Chujo, Y.; Hanrath, T.; Ober, C. K.; Wise, F. W. Role of Solvent Dielectric Properties on Charge Transfer from PbS Nanocrystals Molecules. *Nano Lett.* **2010**, *10*, 318–323.
53. Bian, K.; Choi, J. J.; Kaushik, A.; Clancy, P.; Smilgies, D.-M.; Hanrath, T. Shape-Anisotropy Driven Symmetry Transformations in Nanocrystal Superlattice Polymorphs. *ACS Nano* **2011**, *5*, 2815–2823.
54. Lee, S. M.; Jun, Y. W.; Cho, S. N.; Cheon, J. Single-Crystalline Star-Shaped Nanocrystals and Their Evolution: Programming the Geometry of Nano-Building Blocks. *J. Am. Chem. Soc.* **2002**, *124*, 11244–11245.
55. Lu, W. G.; Fang, J. Y.; Ding, Y.; Wang, Z. L. Formation of PbSe Nanocrystals: A Growth toward Nanocubes. *J. Phys. Chem. B* **2005**, *109*, 19219–19222.
56. Choi, J. J.; Luria, J.; Hyun, B.-R.; Bartnik, A. C.; Sun, L.; Lim, Y.-F.; Marohn, J. A.; Wise, F. W.; Hanrath, T. Photogenerated Exciton Dissociation in Highly Coupled Lead Salt Nanocrystal Assemblies. *Nano Lett.* **2010**, *10*, 1805–1811.
57. Kaushik, A. P.; Clancy, P. Solvent-Driven Symmetry of Self-Assembled Nanocrystal superlatticesA Computational Study. *J. Comput. Chem.* **2013**, *34*, 523–532.
58. Liu, Y.; Gibbs, M.; Puthussery, J.; Gaik, S.; Ihly, R.; Hillhouse, H. W.; Law, M. Dependence of Carrier Mobility on Nanocrystal Size and Ligand Length in PbSe Nanocrystal Solids. *Nano Lett.* **2010**, *10*, 1960–1969.
59. Choi, J. J.; Bealing, C. R.; Bian, K.; Hughes, K. J.; Zhang, W.; Smilgies, D.-M.; Hennig, R. G.; Engstrom, J. R.; Hanrath, T. Controlling Nanocrystal Superlattice Symmetry and Shape-Anisotropic Interactions through Variable Ligand Surface Coverage. *J. Am. Chem. Soc.* **2011**, *133*, 3131–3138.
60. Frisch, M. J.; Trucks, G. W.; Schlegel, H. B.; Scuseria, G. E.; Robb, M. A.; Cheeseman, J. R.; Scalmani, G.; Barone, V.; Mennucci, B.; Petersson, G. A.; *et al.* Gaussian *09*; Gaussian, Inc.: Wallingford, CT, 2009.
61. Sini, G.; Sears, J. S.; Bredas, J.-L. Evaluating the Performance of DFT Functionals in Assessing the Interaction Energy and Ground-State Charge Transfer of Donor/Acceptor Complexes: Tetrathiafulvalene-Tetracyanoquinodimethane (TTF-TCNQ) as a Model Case. *J. Chem. Theory Comput.* **2011**, *7*, 602–609.